This article has been accepted for publication in a future issue of this journal, but has not been fully edited. Content may change prior to final publication. Citation information: DOI 10.1109/JESTPE.2017.2751745, IEEE Journal of Emerging and Selected Topics in Power Electronics

Design and Optimization Techniques of Over-Chip Bondwire MicroTransformers with LTCC core

Antonio Camarda, Enrico Macrelli, *Member, IEEE*, Rudi Paolo Paganelli, Marco Tartagni, *Member, IEEE*, Saibal Roy, *Member, IEEE*, Aldo Romani

***Abstract*— This paper describes the realization of bond-wire micro-magnetics by using standard bonding-wires and a toroidal ferromagnetic LTCC core with high resistivity. The proposed fabrication procedure is suitable for the development of magnetic components on top of an IC with small profile and small size (< 15 mm^2). A transformer is designed and applied over-chip, working in the MHz range with high inductance (~33 µH) and high effective turns-ratio (~20). Applications include bootstrap circuits and micro-power conversion for energy harvesting. Measurements demonstrate a maximum secondary *Q*-factor of 11.6 at 1.3 MHz, and a coupling coefficient of 0.65 with an effective turns ratio of 19, which are among the highest values reported for toroidal miniaturized magnetics. The achieved inductance density is 2 µH/mm^2, along with an inductance per unit core volume of 15.6 µH/mm^3, and a DC inductance-to-resistance ratio of 2.23 µH/Ω. The presented technique allows to obtain over-chip magnetics trough a post-processing of the core, and it is also suitable for high-density power supply in package (PwrSiP) and power supply on chip (PwrSoC). Finally, a series of optimization techniques for planar core magnetic devices in order to maximize the inductance per unit area are discussed and applied to the considered case.**

***Index Terms*— bonding wire, ferrite, harvesting, on-chip, over-chip, low-temperature co-fired ceramic, magnetic transformer, power supply in package (PwrSiP), power supply on chip (PwrSoC).**

I. Introduction

THE ongoing miniaturization of electronic products is placing significant challenges on power converters and energy harvesting (EH) systems. A major task is related to the development of micro-magnetic components compatible with integrated circuit (IC) processes with performance similar to discrete counterparts [1]. Additionally, the market is increasing the interest for the realization of monolithic platforms generally known as power supply in package (PwrSiP) and power supply on chip (PwrSoC).

Although battery-powered systems are common in electronic devices, batteries are not tolerable for wearable and bio-implantable systems as maintenance is hard [2]. A possible solution is to extract energy from the environment as in micro- and milli-power EH systems. Among them, thermoelectric generators (TEGs) often output very low voltages down to few tens of mV. In this case, a battery-less EH system, besides power conversion, requires dedicated bootstrap circuits in a footprint of few mm^2 [2] [3] with magnetic components as building blocks. However, on-chip magnetic devices cannot be easily miniaturized likewise microelectronic circuits. Hence, the size reduction of micro-magnetic devices represent an existing challenge for EH circuits, which presently require external passives [2] [4] [5].

Designing micro-inductors and micro-transformers for valuable inductance values in available sizes and acceptable efficiency is a demanding task [1]. At very high switching frequencies (>50MHz), the value of the required inductance is compatible with air-core inductors with several limitations associated with technical performance. More precisely, the absence of a magnetic core worsens the overall power system efficiency, given that at such very high frequency, the magnetic field of an air-core inductor can couple with the substrate of an IC thus causing a latch-up or an unpredictable behavior of the underlying circuit [6] [7].

Generally, spiral air-core inductors are directly manufactured in standard IC processes exploiting the metallization embedded in the technology. However, air-core inductors achieve low coupling and low inductances. On the other hand, magnetic-core components permit higher energy storage and higher inductances with the drawback of higher power losses due to hysteresis and eddy currents, and core saturation [8]. For instance, in [9] a comparison between 36 nH magnetic- and air-core spiral inductors is described showing

This paragraph of the first footnote will contain the date on which you submitted your paper for review.

Special Issue on Power Supplies on Chip, (PwrSoC), 2016.

(*A. Camarda and E. Macrelli contributed equally to this work*). (*Corresponding authors: A. Camarda; E. Macrelli*)

A. Camarda, A. Romani and M. Tartagni are with the Advanced Research Center on Electronic Systems of the University of Bologna, 47521 Cesena, Italy. (e-mail: antonio.camarda@unibo.it, marco.tartagni@unibo.it, aldo.romani@unibo.it).

E. Macrelli was with the Advanced Research Center on Electronic Systems of the University of Bologna, 47521 Cesena, Italy. He is now with the Dept. of Electrical & Computer Engineering of the National University of Singapore, 117583 SGP (e-mail: enrico.macrelli@nus.edu.sg).

R. P. Paganelli is with the National Research Council CNR-IEIIT, c/o University of Bologna, 40136 Bologna, Italy (e-mail: rudipaolo.paganelli@cnr.it).

S. Roy is with the Micro-Nano Systems Centre of the Tyndall National Institute and with the Department of Physics, University College Cork, Cork T12 R5CP, Ireland (e-mail: saibal.roy@tyndall.ie).

This article has been accepted for publication in a future issue of this journal, but has not been fully edited. Content may change prior to final publication. Citation information: DOI 10.1109/JESTPE.2017.2751745, IEEE Journal of Emerging and Selected Topics in Power Electronics

that the performance of the magnetic core inductor is superior up to 50 MHz. However, on-chip magnetics typically require complex and costly deposition methods that restrict their application market [1].

To pursue miniaturization, device integration can be achieved through various levels: wafer, package and board [10]. Package integration means that the magnetics are co-packaged with the die and connected within the package; wafer integration means that the magnetics are built on-chip, or over the chip (as post-processing step), minimizing the overall area usage; board integration means that the magnetics are fabricated on a substrate where the active part can be mounted.

Generally, as reported in [11], toroidal magnetics are the best solution for step-up transformers with wafer or package integration due to the high DC performance and to the high achievable coupling in a small device area. A simple approach to realize a toroidal power device is based on standard IC bonding wires as top conductors [4] [12]. In terms of quality (Q)-factor and L/R_{DC} (inductance to low frequency resistance ratio), these devices, denoted as bond-wire magnetics [13] - [16], permit performances comparable to integrated, silicon-embedded or drop-in magnetics for power conversion applications with high thickness metallization [15] -[19].

The growing demand for integrated micro-magnetics has encouraged the development of magnetic core materials for power devices, with the aim of increasing inductance as well as of enhancing the coupling between the coils. The most used soft magnetic materials are [1] [7]: iron alloys (FeSi), nickel-iron alloys (NiFe), cobalt-nickel alloys (CoNi), ferrites (MnZn and NiZn), powders, and amorphous (CoFeSi) or nanocrystalline alloys. Low-temperature co-fired ceramics (LTCCs) based on green tapes are widely used to fabricate embedded structures, i.e. conductors, resistors and capacitors, depending on the tape properties and on the manufacturing process [20]. Nowadays, ferromagnetic LTCCs are available with high resistivity and high permeability, opening new prospects in the development of magnetic components for high-frequency applications with low losses [18] [19]. LTCC can be laminated to allow a larger core thickness compared to on-chip deposition techniques [1] [18] [19], at the cost of high sintering temperature

This paper will get in depth into the realization of bond wire micro-magnetics, i.e. inductors and transformers, with multiple windings by using conventional IC bonding wires and magnetic LTCC cores with toroidal race-track shaped patterns. More precisely, the paper investigates a fabrication procedure for bond wire transformers suitable for integration on-top of an IC, thus allowing the design of magnetic devices at silicon die level with a small profile and limited footprint area. According to specific application requirements, the performance of the device can be adjusted by varying the core thickness (and the wire loop height accordingly), and by combining multiple parallel bond-wires to account different levels of current or parasitic resistance [4].

The described micro-fabrication of a ferromagnetic LTCC core is capable of achieving high permeability and large thickness. The proposed technique develops further devices appropriate for operation in a frequency range between 100 kHz and 5 MHz with high inductance and high turns ratio. The $1 : n_2$ (1 turn at the primary and n_2>>1 at the secondary side) design targets to maximize the turns ratio, i.e. the voltage step-up ratio, in a fixed area, whereas the toroidal geometry facilitates high DC inductance to resistance ratios, i.e. ~3μH/Ω and high inductance per unit area, up to ~2 μH/mm^2, key figures of merit for DC performance of micro-magnetics [1] [9]. With respect to an air-core solution, which generally produces a magnetic field component perpendicular to the substrate, a toroidal structure produces a lower external magnetic field coupled with the substrate [21], thus leading also to lower noise in the potential integrated active circuitry below the magnetics. Furthermore, the fabricated magnetics enable the evolution of miniaturized energy autonomous bootstrap circuits and micro-power EH applications [5].

As an additional contribution, this work presents some optimization techniques suitable for planar core-based inductors and transformers: first a more accurate numerical expression for the evaluation of the magnetic path length is presented. This expression is then used within the classic analytical expression for the evaluation of the inductance of a toroidal inductor, in order to find the critical parameters affecting the inductance value once the core footprint area has been fixed. As a conclusion of the work, a new serpentine layout for the core is presented. Such layout allows having a higher inductance/footprint area ratio with respect to the optimized planar toroid.

The manuscript is organized as follows: Section I introduces the paper and gives an overview on the state-of-art of miniaturized magnetics. In section II the layout design and fabrication details of the ferromagnetic LTCC core are reported along with the assembly procedure of the bond wire devices. In section III the DC and AC analytical modeling are illustrated together with the DC results. In section IV the experimental measurements are described together with the performance in comparison with commercial solutions. In section V the optimization techniques are presented, whereas section VI concludes this work.

II. Design and Fabrication

This section shows the layout design of the bond wire transformer on a standard silicon CMOS substrate. Therefore, the fabrication of the magnetic LTCC [22] core is reported along with the assembly procedure of the devices.

A. Layout Design on Silicon Substrate

The proposed transformer is made up of two windings with n_1 and n_2 turns for the primary and secondary side, respectively. The bottom conductors of the coils are composed of the last thick metal layer of a CMOS microelectronic process (see Fig. 1a), whereas the top conductors are completed by using gold bond-wires. The thick metal is made of aluminum-copper (AlCu) with thickness $t_m = 3.2$ μm and sheet resistance $R_{sheet} = 10$ mΩ/□, hence the overall resistance is calculated as $R_m = R_{sheet}\, l_m / w_m$ where l_m and w_m are the length and width of the metallization. We can further extract the metal resistivity as $\rho_m = R_{sheet}\, t_m = 3.2$ μΩ·cm.

In our case, the $1 : n_2$ transformer layout is designed to maximize the turns ratio $n_{12} = n_2 / n_1$ in a footprint area of $A_r = 15$ mm^2. In order to meet the area constraints, the layout is realized with a metal width of $w_m = 90$ μm and a spacing of $s_m = 20$ μm, in accordance to the constraints of the IC technology, and a bond pad pitch (BPP) of 112 μm, thus

This article has been accepted for publication in a future issue of this journal, but has not been fully edited. Content may change prior to final publication. Citation information: DOI 10.1109/JESTPE.2017.2751745, IEEE Journal of Emerging and Selected Topics in Power Electronics

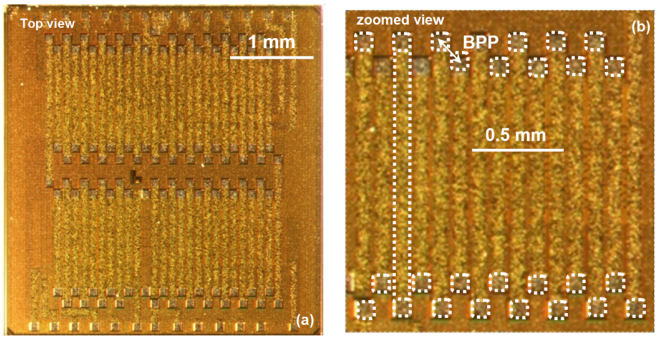

Fig. 1. Microphotographs of the designed IC with the thick metal of the CMOS process visible (a) and of a particular with design parameters associated to the layout (b). In Fig.1b the pads are highlighted as well as single metal turn.

obtaining a 1 : 50 turns transformer, i.e. $n_{12} = 50$. This design optimization along with the choice of the $1 : n_2$ turns ratio, allow the transformer to achieve a high voltage ratio useful for reducing the minimum activation voltage of a bootstrap circuit for use in battery-less micro-power EH applications [2] [4] [5]. Other applications such as power conversion may benefit from different turn ratios. The minimum outer and inner pad distances from the magnetic core are set to d_{ext} = 450 µm and d_{int} = 225 µm, respectively, with zig-zag pads [23] in order to increase the yield in wire bonding process and to maximize n_{12} while complying with the minimum BPP. The above geometrical quantities are depicted in Fig. 1b.

B. Fabrication of the magnetic LTCC core

The ferromagnetic LTCC core is fabricated starting from the commercial green tape ESL-40012 from ElectroScience [20] [24] [25], which is a flexible cast film of magnetic powder designed to be sintered at very high temperatures (up to 1200°C). This allows to obtain an isotropic ceramic core and to get large grains thus achieving considerable magnetic properties. Table I reports the main properties of the 40012 LTCC magnetic tape as stated by the manufacturer [25], however it is worth remarking that magnetic properties of the ESL 40012 such as permeability, firing-temperature dependence, magnetization, and coercive field were already reported [20], [26]-[30]. Moreover, it is worth noting that the permeability of this material strictly depends on the sintering temperature [30].

The fabrication of the magnetic LTCC core (Fig. 2a) involves three micro-fabrication stages: lamination (steps 1-2-3), cutting (step 4), and firing (step 5). At the end (step 6), the LTCC core is obtained. In the lamination step $n_l = 9$ layers of green tapes of thickness t_l are stacked with a warm isostatic press (Jenoptik Hot Embosser) at a pressure of 14 MPa and temperature of 70°C. This step allows increasing the core cross-section as well as the self-inductances of both coils. We chose 9-layers in order to limit the overall core thickness to 0.4 mm to reduce the profile of the device. The press applies first high pressure and then the sample is cooled to get a single stack. In the next step, the stack is cut in a toroidal race-track shaped pattern with a laser equipment. In the sintering step the cut sample is fired in a muffle furnace (Nannetti KL 20). During the firing step, the dimensions of the sample shrank because of frictional forces, however this shrinkage can be compensated during the design phase in order to achieve the desired size at end of the process.

TABLE I. ELECTRICAL AND MAGNETIC PROPERTIES OF THE 40012 LTCC MAGNETIC TAPE

Supplier	ESL
Material	magnetic LTCC
Part number	40012
ρ_e (Ω cm) [29]	~50 (estimated)
t_l (µm) [24]	60
μ_{rc} (after firing) [26]-[29]	~400-500
H_c (A m^{-1}) [26]	330
B_s (mT) [26]	~400
B_r (mT) [26]	250

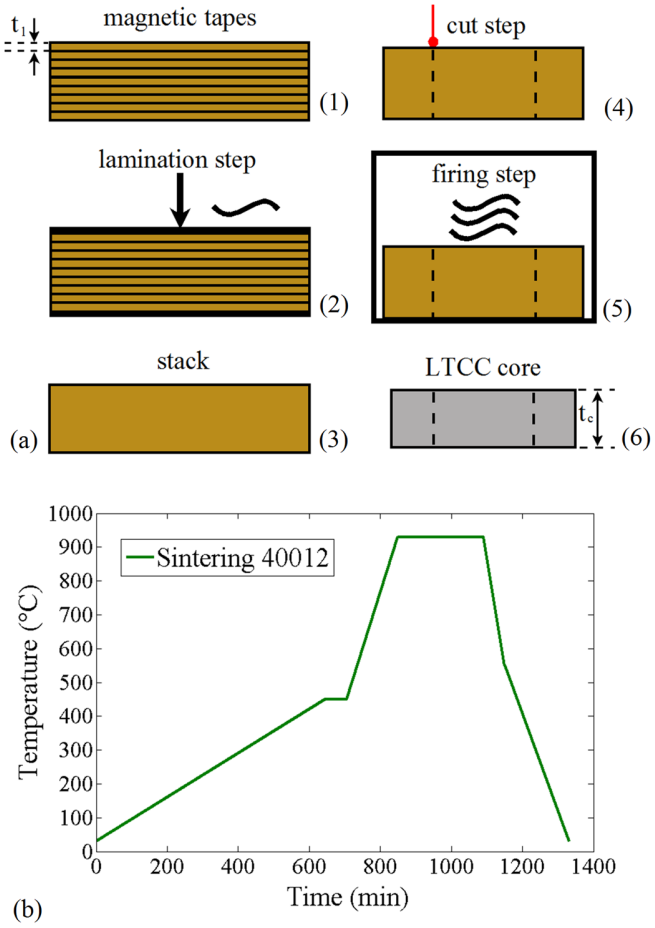

Fig. 2. Micro-fabrication steps of the ferromagnetic LTCC core (a) and sintering stages performed in a muffle furnace (b).

The sintering phase comprises the following temperature profile (Fig. 2b): i) the temperature is ramped with a slope of 0.7°C/min from room temperature up to 450°C , ii) hold at 450°C for 1 hour, iii) ramped with a slope of 3.5°C/min from 450°C to 930°C, iv) hold at peak value for 4 hours, v) ramped down with a negative slope of -6.3°C/min from 930°C to 550°C, vi) cooled down to room temperature (slope ~3°C/min). The fabricated magnetic LTCC core has a ceramic body with a measured thickness of $t_c \cong 390$ µm, a relative permeability of $\mu_{rc} \cong 500$ (from datasheet) and a measured shrinkage of 20% in all directions, in accordance with the data provided by the manufacturer. Fig. 3 shows two

This article has been accepted for publication in a future issue of this journal, but has not been fully edited. Content may change prior to final publication. Citation information: DOI 10.1109/JESTPE.2017.2751745, IEEE Journal of Emerging and Selected Topics in Power Electronics

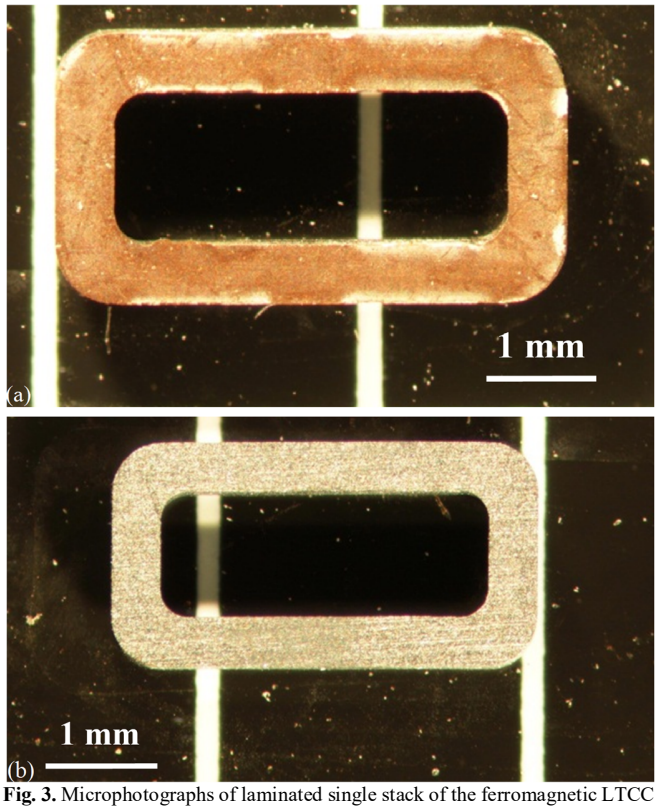

Fig. 3. Microphotographs of laminated single stack of the ferromagnetic LTCC core before (a) and after (b) the firing step.

microphotographs of the laminated single stack before (top picture) and after (bottom picture) the sintering phase.

C. Assembly of the device

The transformer is assembled with a Kulicke & Soffa (K&S) 8208-PPS wire bonder with gold round wires (diameter $d_b = 25$ µm and resistivity $\rho_b \cong 2.44 \cdot 10^{-6}$ Ω·cm) with the LTCC core mounted on-top of the IC. The passivation layer deposited on top of the last metal layer at the end of the silicon process ensures the isolation between the core and the conductors. Moreover, the core was manually aligned on top of the die and glued with an epoxy-resin paste. The fabricated device has the following characteristics: core size $3.8 \times 2.0 \times 0.5$ mm^3 ($l \times p \times w_c$, see Fig. 4), core cross-section $A_c \cong 0.20$ mm^2, core mean magnetic path length (MPL) $l_c \cong 9.6$ mm, core volume $V_c = A_c \cdot l_c \cong 1.92$ mm^3, metal length per turn (MLT) $l_m \cong 1.32$ mm, and wire MLT $l_b \cong 3.0$ mm. For the presented device, we chose n_1=1 and n_2=50, thus n_{12}= n_2/n_1=50/1. The achieved low-frequency values of L_{11} and L_{22} are ~30 nH and 31 ~µH respectively. Fig. 4 illustrates a microphotograph of the assembled bond wire transformer.

III. Analytical Modeling

This section shows a brief low-frequency as well as a high-frequency analytical modeling of the two-winding bond-wire transformer.

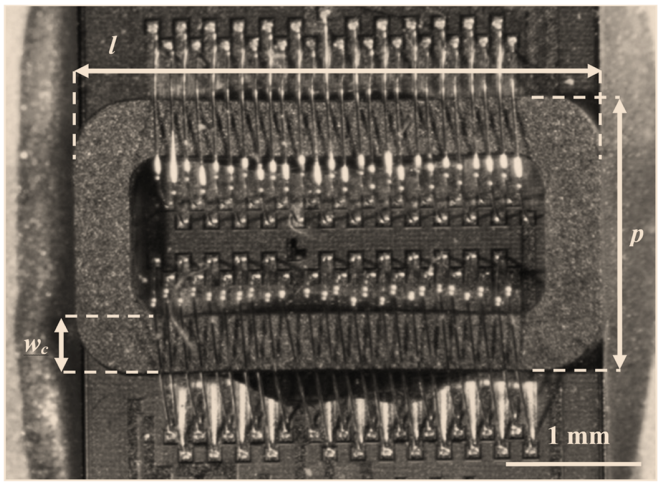

Fig. 4. Microphotograph of the bond wire transformer assembled with magnetic LTCC core and gold bonding wires with dimensions associated to

A. Low-frequency Modeling

The small-signal DC self-inductances of the coils L_{11}^{LF}, L_{22}^{LF} for the magnetic-core transformer are calculated by the reluctance formula ($\Re$) as:

$$L^{LF} = \frac{n^2}{\Re} = \frac{\mu_0 \mu_{rc} n^2 A_c}{l_c} = \frac{\mu_0 \mu_{rc} n^2 t_c w_c}{2(l + p - 2w_c)}, \quad (1)$$

where $A_c = t_c\, w_c$ and $l_c = 2\,(l + p - 2\, w_c)$ with l, p, and w_c as the core length, depth and width as shown in Fig. 4. The coefficient $\mu_0 = 4\pi \cdot 10^{-7}$ H/m represents the free-space permeability and n is the number of turns of the winding considered.

The low-frequency winding resistances of the coils R_{w1}^{LF}, R_{w2}^{LF} are calculated by multiplying by n the resistance of a single turn made by of the resistance of a single bonding-wire R_b^{LF} and that of a single metal R_m^{LF}, as:

$$R_w^{LF} = n(R_b^{LF} + R_m^{LF}) = n\left(\frac{\rho_b l_b}{\pi (d_b/2)^2} + \frac{\rho_m l_m}{w_m t_m}\right). \quad (2)$$

The effective turns ratio n_{eff} is given by:

$$n_{eff} = k\sqrt{L_{22}/L_{11}}, \quad (3)$$

with $k = L_{12}/(L_{11}\,L_{22})^{1/2}$, $0 \le k \le 1$, as the coupling coefficient with L_{12} as the mutual inductance. For an almost-perfectly coupled transformer ($k \cong 1$) the effective turns ratio would become $n_{eff} \cong n_{12}$.

In order to prevent core saturation, the ampere-turn limit for the transformer is given by [7]:

$$(n_1 I_1 + n_2 I_2) \le I_{\max} = \frac{B_s l_c}{\mu_0 \mu_{rc}}. \quad (4)$$

where B_s is the saturation flux density, I_{max} is the equivalent saturation current (or maximum equivalent magnetomotive force given by the product of the current times the turns number), while I_1 and I_2 are the amplitudes of the currents flowing in the coils.

If we consider a sinusoidal waveform applied to the primary coil with the secondary open, the minimum frequency $f_{\min}$ for preventing saturation is derived directly from the Faraday' s law of electromagnetic induction:

This article has been accepted for publication in a future issue of this journal, but has not been fully edited. Content may change prior to final publication. Citation information: DOI 10.1109/JESTPE.2017.2751745, IEEE Journal of Emerging and Selected Topics in Power Electronics

$$f_{\min} = \frac{V_{1\max}}{2\pi n_1 A_c B_s}, \quad (5)$$

where $V_{1\max}$ is the peak voltage amplitude of the waveform applied. If a square-wave is applied to the device, as it happens in magnetic-based switching power converters, then the factor 2π in (5) should be replaced by the factor 4 [7].

Table II summarizes the modeling results of the DC analysis of the bond wire devices. The magnetic LTCC core provides an improvement higher than 100X the L_{22} of the epoxy air-core device, with a $I_{max} \cong 4.9$ A which results in $I_1 \cong 4.9$ A with the only primary coil (i.e. $I_2 = 0$ A), and in a $f_{min} = 246$ kHz obtained at $V_{1max} = 100$ mV, which is the typical target input voltage for bootstrap circuits. However, the DC or RMS current in gold bonding wires with $d_b = 25$ µm is recommended to be lower than about 0.62 A [31] for preventing damage.

B. High-frequency Modeling

At higher frequencies, the current flowing in a coil produces a magnetic field inducing the skin effect in the conductor due to opposing eddy currents. The time-varying magnetic field in the LTCC core self-induces a voltage that generates circulating currents and so power losses, which can modelled by introducing a complex magnetic permeability $\mu(f) = \mu_{rs}'(f) - j\mu_{rs}''$. Hence, the small-signal self-inductances of the coils L_{11}, L_{22} for the magnetic-core device are calculated by the series complex permeability model [7] as:

$$L = L_0^{LF}\mu_{rs}' = \frac{L_0^{LF}\mu_{rc}}{\sqrt{1+(f/f_H)^2}}, \quad (6)$$

where $L_0{}^{LF}$ is equal to the low-frequency self-inductance from (1) normalized against μ_{rc}, whereas f_H is the cut-off (-3dB) frequency of the inductive relative permeability μ_{rs}' due to skin effect and is equal to [32]:

$$f_H = \frac{4\rho_c}{\pi\mu_0\mu_c t_c^2}, \quad (7)$$

where ρ_c represents the core resistivity. Equation (7) further represents the frequency at which the skin depth is equal to $t_c/2$. We recall that the expression of the skin depth for both the core and the metal is expressed as [7]:

$$\delta_{b,c} = \sqrt{\frac{\rho_{b,c}}{\pi\mu_0\mu_{b,c}f}}, \quad (8)$$

Equation (6) generally is applicable for most of ferrite compounds. Similarly, the small-signal core equivalent series resistance (ESR) R_c due to skin effect is calculated as [7]:

$$R_c = 2\pi f L_0^{LF}\mu_{rs}'' = \frac{2\pi f L_0^{LF}\mu_{rc}}{\sqrt{1+Q^2(f/f_H - f_H/f)^2}}, \quad (9)$$

where $Q = f_H/\Delta f$ is the quality factor with Δf(Hz) being the -3dB bandwidth of the resistive relative permeability μ_{rs}'' estimated to be $\Delta f = 1.6$ MHz. By considering the skin effect in the conductor, the small-signal winding resistances R_{w1}, R_{w2} are obtained by adding the AC resistances of a single round bonding wire R_b and of a single metal R_m multiplied by n as:

TABLE II. MODELING RESULTS OF THE DC ANALYSIS OF THE BOND WIRE TRANSFORMER

Core	LTCC
$L_{11}{}^{LF}$ (nH)	12.8
$L_{22}{}^{LF}$ (µH)	30.8
$R_{w1}{}^{LF}$ (Ω)	0.30
$R_{w2}{}^{LF}$ (Ω)	14.8
$I_{\max}$ (A)	4.9
f_{min} (kHz) @ 100 mV	246

$$R_w = n(R_b + R_m) = n\left(\frac{\rho_b l_b}{\pi\delta_b(d_b - \delta_b)} + \frac{\rho_m l_m}{2\delta_m w_m}\right), \quad (10)$$

where δ_m and δ_b are the skin depths of metals and bonding wires, respectively. Nevertheless, (10) is an approximation valid for conductor thicknesses higher than 3δ and does not account for proximity effects, which can be as important as skin depth effects [7].

Fig. 5 depicts the normalized resistance variation against the frequency due to skin effect, obtained through Finite Element Method (FEM) simulations, for a gold bond-wire with 25 µm of diameter ($\sigma_b \cong 4.1\cdot10^7$ S/m). The resistance variation can be assumed to be negligible for frequencies up to 30 MHz, where the resistance is about 1.7 times the DC resistance. Now, we can extract the small-signal AC series resistances R_{11}, R_{22} as:

$$\begin{aligned} R_{11} &= R_{w1} + R_c \\ R_{22} &= R_{w2} + R_c n_{12}^2 \end{aligned}, \quad (11)$$

The AC total core power losses per unit volume P_v (mW/cm^3), due to hysteresis and eddy currents effects is given by [7]:

$$P_v = \frac{P_c}{V_c} = \frac{R_{cc}I_{rms}^2}{V_c} = \frac{R_c}{V_c}\cdot\frac{1}{2}\left(\frac{l_c B_m}{\mu_0\mu_{rc}n_1}\right)^2, \quad (12)$$

where P_c is the total core loss, V_c is the core volume in cm^3, $I_{rms} = (l_c B_m)/\sqrt{2}(\mu_0\mu_{rc}n_1)$ is the rms current applied on the primary coil with B_m as the amplitude of the induced AC magnetic flux density and R_{cc}=$R_c + R_h$, with R_h the equivalent resistance taking into account the hysteresis losses. Equation (12), has a general validity. In case of small-signals (linear region of the device) we have $R_{cc} \cong R_c$. Generally, power losses can be described by the Steinmetz Equation (SE):

$$\langle P_v(t)\rangle = kf^\alpha B_m^\beta \quad (13)$$

where $\langle P_v(t)\rangle$ is the average power loss for a sinusoidal waveform, and k, α and β are the parameters of the magnetic material considered generally provided by manufacturers. The value of α is normally between 2 and 3 [7]. However, (13) is valid only for a sinusoidal waveform, and the characteristic parameters of the SE are valid only in a small frequency range. Moreover, losses are a non-linear phenomenon, hence in order to evaluate the losses in a switching converter driven by a square-wave it is not possible to apply a Fourier-series decomposition [33] [34].

Fig. 6 depicts the numerically estimated skin depths compared with sizes t_c and d_b for the presented transformer. The high resistivity of the LTCC tape ($\rho_c \sim 50$ Ω·cm was estimated

This article has been accepted for publication in a future issue of this journal, but has not been fully edited. Content may change prior to final publication. Citation information: DOI 10.1109/JESTPE.2017.2751745, IEEE Journal of Emerging and Selected Topics in Power Electronics

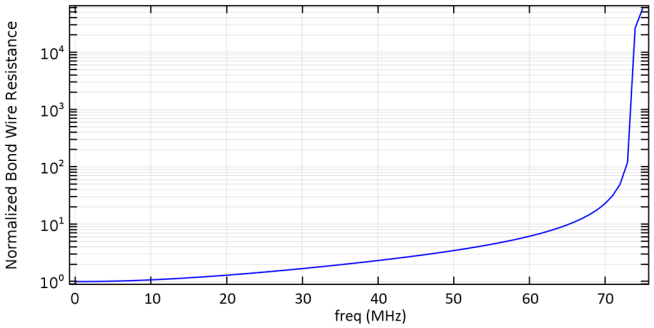

Fig. 5. Normalized resistance R_b obtained through FEM simulation of a gold bond-wire with d_b=25 µm and σ_b =1/ρ_b = 4.1·10^7 S/m. The resistance does not show considerable variations up to 30MHz.

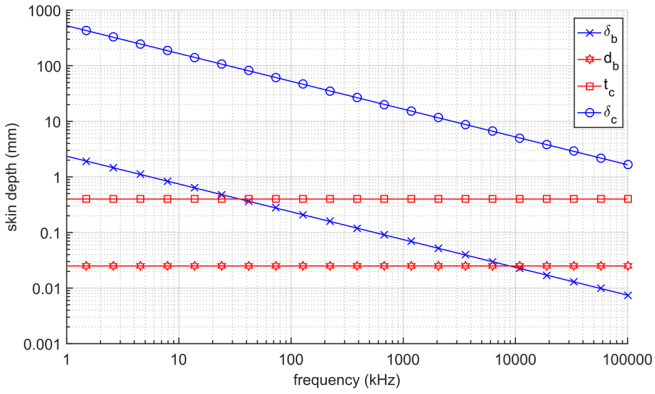

Fig. 6. Comparison between calculated skin depths δ_c and δ_b and sizes t_c and d_b as a function of frequency for the bond wire transformer with LTCC core.

from [29] and reported in Table I) leads to a large core skin depth δ_c compared to the core thickness (i.e. $\delta_c >> t_c$), meaning negligible eddy-current losses in the core, whereas high-frequency effects arise in the bonding wires beyond 7 MHz ($\delta_b \approx d_b$). It is worth remarking that both analytical and FEM simulations do not account for anomalous losses (also known as excess eddy currents losses-ECL), given that such losses cannot be modeled by only exploiting classic Maxwell equations. ECL are experimentally obtained by difference between the actual measured losses and analytically estimated of the eddy currents losses [34] - [36].

IV. Measurements and Discussion

Measurements were performed using a precision E4980A LCR Meter in order to characterize the device from 10 kHz to 2 MHz, along with a performance comparison with commercial devices. The transformer impedances $Z_{11} = R_{11} + j\,2\pi f L_{11}$ and $Z_{22} = R_{22} + j\,2\pi f L_{22}$ are measured from the two-port network by performing standard open- and short-circuit tests [7], whereas the mutual inductance L_{12} is measured with series-coupling tests [37]. Therefore, the coupling coefficient k and the effective turns ratio n_{eff} from (3) are extracted, along with the Q-factors given by $Q_{11} = 2\pi f L_{11} / R_{11}$ and $Q_{22} = 2\pi f L_{22} / R_{22}$.

Fig. 7 depicts the comparison between the predicted and measured L_{11} and L_{22}, whereas Fig. 8 presents the numerically estimated and measured values of R_{11} and R_{22} of the LTCC core device. The predicted value of L_{22} obtained from (6) agrees with measurements, as well as the calculated series resistances

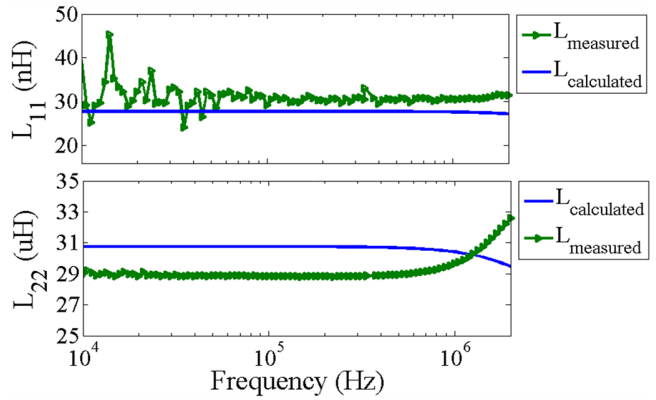

Fig. 7. Comparisons between calculated and measured L_{11} and L_{22} as a function of frequency of the LTCC core transformer obtained with open- and short-circuit tests.

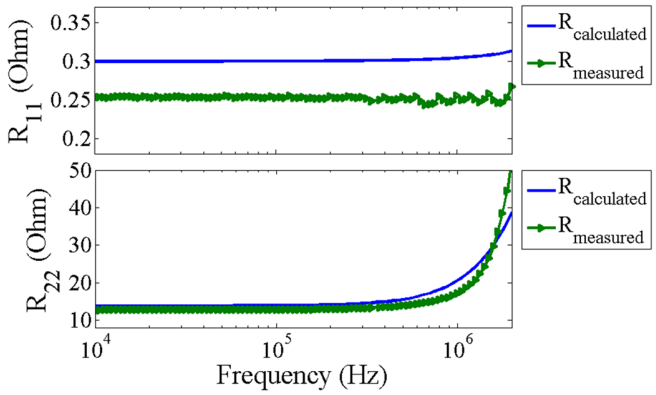

Fig. 8. Comparisons between calculated and measured R_{11} and R_{22} as a function of frequency of the LTCC core transformer.

obtained from (10). The calculated L_{22} includes further the estimated inductance (~15 nH) of the bonding wires used to connect the pads from die to package. The high-frequency increase in R_{22} starting from 1 MHz is attributed mainly to hysteresis losses and ECL in the magnetic core. The results show that the ferromagnetic LTCC core improves L_{22} to 29 µH (with a peak value of 33 µH) with a low frequency R_{22} of ~13 Ω. An inductance per unit area as high as ~2 µH/mm^2 at low frequency is obtained, which is one of highest values reported in literature for over-chip (including also on-chip) inductors, together with an inductance per unit core volume of ~15.6 µH/mm^3, whereas the inductance to DC resistance ratio is 2.23 µH/Ω which is a high value compared to other state-of-the-art devices as in [1].

Fig. 9 shows the measured k and n_{eff} of the LTCC core device, whereas Fig. 10 illustrates the Q_{11} and Q_{22} of the same device. The results show that k (top picture) is enhanced to ~0.65 with a n_{eff} (bottom picture) of about 19, whereas the maximum Q_{22} improves to 11.6 at 1.3 MHz. Hence, the bandwidth of the device is compatible with bootstrap purposes [4] [5] and the achieved inductance value is compatible also with piezoelectric transformers (PTs) based bootstrap circuits, where an inductor is coupled with a PT to further decrease the minimum voltage that can be sensed and boosted [38] – [41]. The inductance of the bonding wires used to connect the device to the package affects the performance by adding an additional leakage inductance in series with L_{11}. The major effect is the decrease

This article has been accepted for publication in a future issue of this journal, but has not been fully edited. Content may change prior to final publication. Citation information: DOI 10.1109/JESTPE.2017.2751745, IEEE Journal of Emerging and Selected Topics in Power Electronics

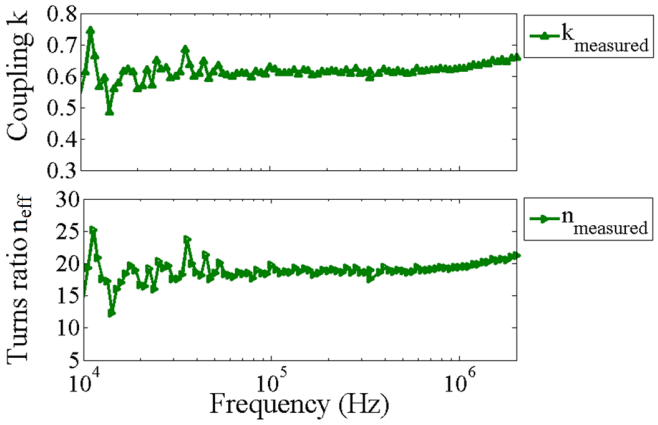

Fig. 9. Measured coupling coefficient k and effective turns ratio n_{eff} as a function of frequency of the LTCC core transformer obtained with series-coupling tests.

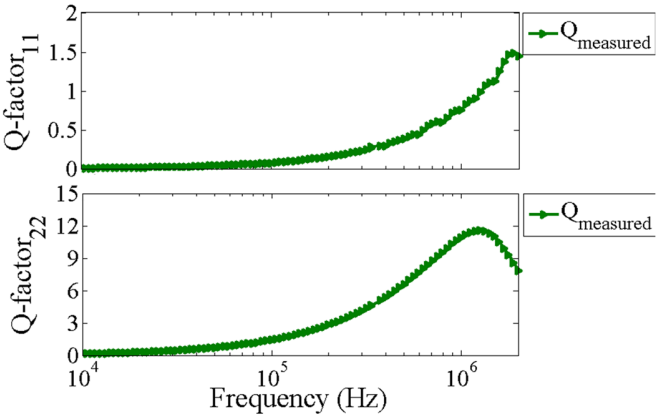

Fig. 10. Measured quality-factors Q_{11} and Q_{22} as a function of frequency of the LTCC core transformer. A maximum Q_{22} of about 11.6 at 1.3 MHz is obtained.

of the value of n_{eff}. This consideration, leads to the conclusion that shorter wires with a global inductance much less than L_{11} should be used in order to improve the effective turns-ratio and the coupling coefficient.

To estimate the AC total core power loss per unit volume P_v described in (12), the R_c values are extracted from the measured R_{22} in Fig. 8 by subtracting the equivalent wires resistance, given that at frequencies below 2 MHz it holds that $R_{w2} \cong R_{w2}^{LF}$, thanks to negligible skin-depth effects in the wires (see Fig.6), thus obtaining $R_c \cong (R_{22} - R_{w2}) / n_{12}^2$. This operation was performed for the following frequencies: 0.5 MHz, 0.7 MHz, 1 MHz and 2 MHz. Fig. 11 shows the numerically estimated P_v of the LTCC core device through (12). To cite an example, the core losses range from 1.94 mW/cm^3 to 90 mW/cm^3 at a magnetic flux density of 10 mT (corresponding to a current of 108mA RMS). All the measurements were performed at 0.1V rms.

By summarizing, the proposed bond wire LTCC core transformer has (at 1.3 MHz): a turns-ratio n_{12} of 50 with $k \cong 0.65$, a self-inductance L_{22} up to ~33 µH (from Fig. 7) and a maximum Q_{22} of 11.6 (from Fig. 10) in a footprint area of about 15 mm^2. As a comparison the performances of the commercial 1 : 10 LPR4012 transformer [42] were measured: it presents (at 850 kHz): a turns ratio n_{12} of 10 (5X lower) with higher $k \cong 0.95$, a self-inductance L_{22} up to 190 µH (6.1X greater) and

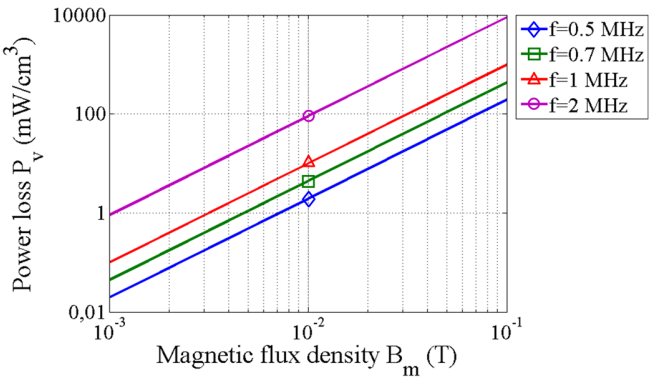

Fig. 11 Calculated power loss density P_v as a function of magnetic flux density for various frequency of the LTCC core transformer.

a maximum Q_{22} of 57 (4.9X greater) in a slightly higher footprint area of ≅ 16 mm^2. Besides, the device in [41] has a higher profile h of 1.1 mm compared to the ~ 0.5 mm of the bond wire device. The commercial discrete provides a saturation current on the primary of ≅ 1.7 A compared to the calculated ≅ 4.9 A from Table II. However, the latter value must comply with the recommended limits (~ 0.62 A) to prevent and eventual damage of wires [31]. Table III illustrates a performance comparison between the proposed bond-wire transformer and the aforementioned commercial discrete samples [42] [43] for low voltage step-up purposes. Although commercial solutions generally have higher inductance value at the cost of higher sizes, the proposed bond wire magnetics are ideal for low voltage step-up circuits directly implementable at die level. As already discussed before, the LTCC has the magnetic permeability strictly dependent on the firing temperature: for higher inductance values, the firing temperature can be augmented to 1030°C, providing relative magnetic permeability up to ~10^3 [30], hence increasing the quality factor at the expenses of a reduced bandwidth.

A solution to improve k is to reduce the wire loop height and pad distances from core, thus minimizing the leakage magnetic flux, and to use shorter wires from die to package. The self-inductances can be increased by using a larger core cross-section, i.e. by increasing w_c and/or t_c, at the cost of higher core losses at high frequency. Nevertheless, it is worth remarking that the LTCC patterning technique allows a high flexibility for the fabrication of miniaturized transformers, given that the final value of the inductance and its performances can be modulated by simply adding more sheets. Another solution for increasing the self-inductance is also the optimization of the layout and this technique is briefly presented in the next section.

Concerning the performances of the device when used for a targeted application, such as the Armstrong oscillator [5], the main performances parameters to assess are the effective turns-ratio n_{eff} (Fig. 9), the coupling factor k (Fig. 9) and the parasitic series resistance at the primary side $R_{11}(f_{OSC})$ as stated in [5], with f_{OSC} the estimated oscillation frequency of the circuit. For this kind of application, a custom design of the oscillator aims at lowering as much as possible the minimum TEG output voltage V_{TEG0} allowing to trigger an oscillation. In fact, V_{TEG0} is inversely proportional to n_{eff}, whereas it increases

This article has been accepted for publication in a future issue of this journal, but has not been fully edited. Content may change prior to final publication. Citation information: DOI 10.1109/JESTPE.2017.2751745, IEEE Journal of Emerging and Selected Topics in Power Electronics

TABLE III PERFORMANCE COMPARISON BETWEEN THE PROPOSED BOND-WIRE DEVICE AND TWO COMMERCIAL TRANSFORMERS FOR LOW VOLTAGE STEP-UP IN MICRO-POWER APPLICATIONS.

Parameter	This device	Coilcraft 1 : 10 [42]	Coilcraft 1 : 10 [43]
n_{12}	50	10	10
k	0.65	0.95	0.95
A_r (mm^2)	15	16	36
h (mm)	0.5[a]	1.1	3.5
L_{22} (μH) @ Q_{max}	31	190	2500
Q_{22}[b](max)	11.6 (@1.3MHz)	57 (@850kHz)	88 @158kHz
I_{max} (A)	≈ 0.62[c]	1.7[d]	1.3[d]
integration	over-chip	discrete	discrete

[a]: without substrate.
[b]: at 0.1 V RMS.
[c]: recommended to avoid wires damage.
[d]: due to core saturation.

as $R_{11}(f_{OSC})$ increases [5]. The effective turns-ratio n_{eff} is strictly dependent on the coupling coefficient k, which in turn can be augmented by increasing the core magnetic permeability μ_{rc}. However, the increase of either t_c or μ_{rc} might lead to higher values of $R_{11}(f_{OSC})$ and hence higher values of V_{TEG0}. We can conclude that there exists a trade-off between the transformer standalone performance parameters and the global boost-oscillator key performance parameters.

V. DESIGN OPTIMIZATION

This section deals with a technique suitable to design the inductance of planar core micromagnetic devices such as the proposed microtransformers. The potential target application is a bootstrap circuit (i.e. Armstrong oscillator) useful to boost the low voltage (tens-hundreds mV) provided by a transducer acting as a harvesting DC source such as thermoelectric generators, rectifying antenna or indoor photovoltaic cells. As stated in [12] - [13], the L_{22} of a microtransformer as well as its n_{12} play an important role for the minimum DC voltage that can be sensed and boosted. The proposed technique, based on geometrical layout considerations, aims at maximizing the inductance per unit area for a fixed footprint area. Hence, the skin depth effects in the core are not accounted, given that the core thickness t_c is not considered a parameter which can modulated, since it puts some important trade-off between the maximum frequency and inductance value.

A. MPL estimation

First, a more accurate analytical expression to evaluate the low-frequency inductance is required. As reported in (1), the inductance value is strictly dependent on the value of the MPL l_c. However, small variations on the determination of l_c might lead to high variations of the final value of the self-inductance.

If we assume for simplicity a square planar toroid, the most-used formula in literature [7] to determine l_c is:

$$l_c = \frac{4(x_A + x_B)}{2} = 4(x_A + w_c) = 4(x_B - w_c), \qquad (14)$$

where x_A and x_B are respectively the lengths of the side of the internal and of the external perimeter (see Fig. 12), and w_c is the width of the core. Equation (14) represents the arithmetic

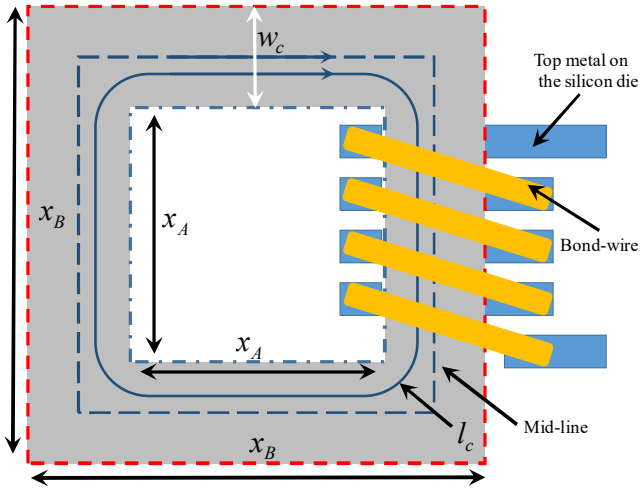

Fig. 12 Example of over-chip bond wire transformer with square planar toroid layout.

average (AA) between internal and external perimeter and assumes a uniform magnetic flux density in the core. Equation (14) simply states that the arithmetic average is given by the contribution of the internal (external) perimeter $P_A = 4x_A$ ($P_B = 4x_B$) plus (minus) the contribution of the four corners $4w_c$.

However, since the magnetic core is folded, the magnetic field density is not uniform in the core cross section, but is much more concentrated close to the internal perimeter [44]. This implies that the geometric average (GA) between the internal and external perimeter $(P_A \cdot P_B)^{1/2}$ can provide a more accurate result with respect to the AA.

A round toroid, with internal radius $r_A = P_A/2\pi$, external radius $r_B = P_B/2\pi$ and core width $w_{cr} = r_B - r_A$ is only subject to the Non-Uniformity (NU) effect. In this case l_c is simply found through averaging of the Ampere's law:

$$l_c(w_{cr}) = \frac{P_A - P_B}{\ln\left(\frac{P_B}{P_A}\right)} = \frac{2\pi w_{cr}}{\ln\left(\frac{P_A + 2\pi w_{cr}}{P_A}\right)} = \frac{2\pi w_{cr}}{\ln\left(\frac{r_A + w_{cr}}{r_A}\right)} \qquad (15)$$

If only the NU is considered for the square toroid, (15) is rewritten as:

$$l_c(w_c) = \frac{P_A - P_B}{\ln\left(\frac{P_B}{P_A}\right)} = \frac{8w_c}{\ln\left(\frac{P_A + 8w_c}{P_A}\right)}. \qquad (16)$$

The magnetic field is not able to follow the right angles of the corner due to a "folding effect" (FE). That means if the core is sufficiently narrow to consider the magnetic field uniform, the contribution of each of the four corners to the overall value of l_c is not w_c, as the AA (14) indicates, but rather $0.56w_c$.

By comparing (15) and (16), we see that l_c can be generically expressed as:

$$l_c(w_c) = \frac{\beta w_c}{\ln\left(\frac{P_A + \beta w_c}{P_A}\right)}. \qquad (17)$$

This article has been accepted for publication in a future issue of this journal, but has not been fully edited. Content may change prior to final publication. Citation information: DOI 10.1109/JESTPE.2017.2751745, IEEE Journal of Emerging and Selected Topics in Power Electronics

If we combine both the NU and FE effects for the square toroid, a value of β that allows to have a qualitative match between (17) and the results given by FEM simulations, is $\beta \cong 5.78$. Hence the effective MPL for a square toroid has the expression:

$$l_c(w_c) \cong \frac{5.78 w_c}{\ln\left(\frac{4x_A + 5.78 w_c}{4x_A}\right)} = \frac{5.78 w_c}{\ln\left(\frac{4x_B - 2.22 w_c}{4x_A}\right)}. \quad (18)$$

Fig. 13 depicts the comparison between AA, GA, NU, Eq. (18), FE, FEM: (18) is the expression providing results closer to the FEM results.

Another consideration worth of attention is that if we compare (15) with (18), we find that a square toroid with external side equal to x_B and footprint area x_B^2 is equivalent, from a reluctance point of view, to a round toroid having $w_{cr}=0.92 w_c$, and internal radius $r_A=2x_A/\pi$. The external radius of the equivalent round toroid is equal to:

$$r_B = \frac{2}{\pi} x_A + 0.92 w_c = \frac{2}{\pi}(x_B - 2w_c) + 0.92 w_c = \cong \frac{2}{\pi} x_B - 0.35 w_c = d_B / 2 \quad (19)$$

with d_b as the external diameter. The equivalent round toroid requires a thickness $t_{cr}=(1/0.92)\cdot t_c=1.087 t_c$ in order to have the same cross section. Hence, the equivalent round toroid (in terms of reluctance) requires a higher thickness and a higher footprint area.

Fig. 14 depicts the comparison between the square toroid and the round toroid: for planar geometries the square allows lower footprint areas compared to equivalent round toroid.

B. *Optimized Square Toroid*

With a more accurate formula it is possible to find the inductance value once the footprint x_B^2 has been fixed. In order to proceed with the analysis, we consider a linear turn density n_0, defined as the average turn per unity length. The inductance in (1) for the square toroid layout then can be written as:

$$L^{LF}(x_B, w_c) = \frac{16 \mu_0 \mu_{rc} x_A^2 n_0^2 t_c w_c}{l_c(w_c)} = = \frac{16 \mu_0 \mu_{rc} (x_B - 2w_c)^2 n_0^2 t_c w_c}{l_c(w_c)} \quad (20)$$

The maximum of (20) is found for:

$$w_c \cong 0.21 x_B. \quad (21)$$

Fig. 15 depicts the behavior of (18). It is possible to demonstrate that with an optimized square toroid, with the same value of n_0, the maximum achievable inductance in 15 mm^2 is around 64 µH, which is a value double than the one achieved in this work.

C. *New layouts*

In addition to the optimization of the square toroid, it is possible to investigate alternative layouts for the core. Even in the optimized square toroid the magnetic field density is not uniform in the core cross-section. If the core is spread all over the surface with a serpentine structure with a narrower width, compared to the square toroid, the magnetic field density is more uniform, and the inductance can be higher if the same

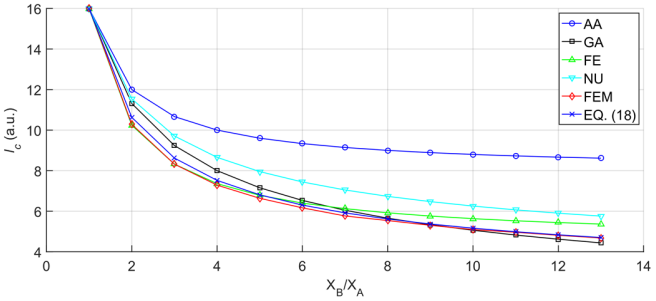

Fig. 13 Comparison between different formulas used to compute the magnetic path length (MPL).

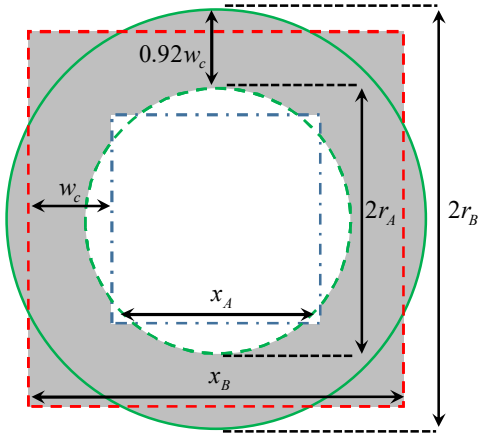

Fig. 14 Geometries comparison between the square toroid and the equivalent round toroid (top view).

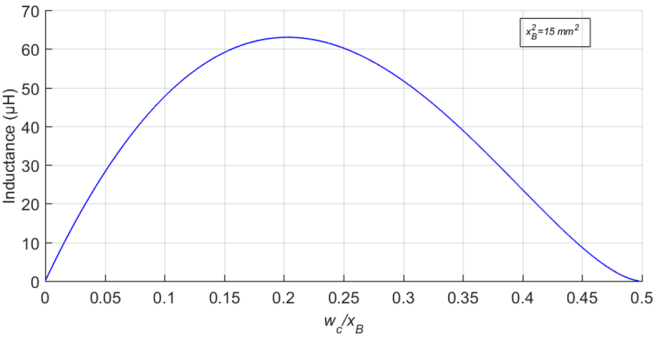

Fig. 15 Inductance of a planar square toroid of 15 mm^2 of footprint area against the core width w_c, made with an LTCC core. The maximum value of inductance is obtained for $w_c=0.21 x_B$.

linear turn density n_0 is considered [44]. If we refer to Fig. 16, we can write:

$$w_c = \frac{(A-G)}{2}$$
$$B = x_B - 2w_c - G \quad . \quad (22)$$
$$A = \frac{x_B - (\alpha/2 - 1)G}{\alpha/2}$$

In (22), α is the number of parallel arms in the y direction. The inductance in this case is written as [44]:

$$L_{SER} \cong \frac{\mu_0 \mu_r t_c w_c n_0^2 \left[P_{INT} - 4(\alpha/2 - 1) w_c\right]^2}{l_c} \quad (23)$$

This article has been accepted for publication in a future issue of this journal, but has not been fully edited. Content may change prior to final publication. Citation information: DOI 10.1109/JESTPE.2017.2751745, IEEE Journal of Emerging and Selected Topics in Power Electronics

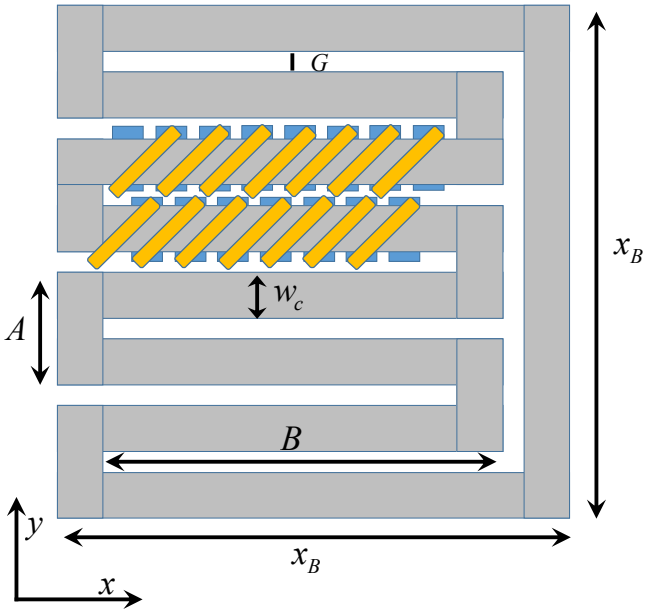

Fig. 16 Serpentine core layout with α=8.

where in (23) P_{INT} is the internal perimeter given by:

$$P_{INT} = 4\left(x_B - 2w_c\right) - \left(\alpha - 2\right)B\,. \tag{24}$$

In (23), we have to consider l_c as the following value [44]:

$$l_c\left(w_c\right) = \frac{5.78w_c}{\ln\left(\frac{P_{INT} + 5.78w_c}{P_{INT}}\right)}. \tag{25}$$

With the developed model, if we assign α=2, we obtain the square toroid (the maximum is obtained for G/x_B=0.58 or w_c/x_B=0.21). From Fig. 17, we see that if we reduce the core width and increase the value of α, it is possible to have an additional increase with respect to the optimized toroid. However, the gap G must be wide enough to allow the winding closure with the wire bonder. Core thickness might also impact on bonding capability, but the serpentine core can bring to higher high-frequency losses due to proximity effects.

VI. Conclusion

This work has investigated the design and fabrication of a bond wire micro-transformer assembled with conventional bonding wires. The prototype is realized on-top of a CMOS IC in a footprint area of 15 mm^2. A ferromagnetic LTCC core has been micro-fabricated as magnetic core starting from green tapes, thus achieving high permeability and proper core section with a small profile of 0.5 mm, and to operate in the MHz frequency range with low losses. Experimental impedance measurements report a secondary self-inductance up to 33 µH with a maximum secondary Q-factor of 11.6 at 1.3 MHz, and a coupling coefficient of 0.65 with an effective turns ratio of 19; some of the highest values in the state-of-the-art for toroidal over-chip magnetics. Calculated core losses range from 1.94 mW/cm^3 to 90 mW/cm^3 at 153 mA of RMS current. From a performance comparison point of view with commercial discrete components, it is worth remarking that the lower profile and the comparable saturation current of the proposed

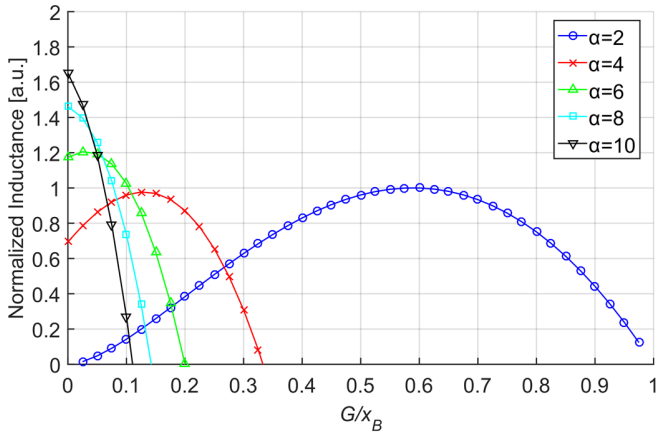

Fig. 17 Normalized Inductance for a serpentine toroid. If α =2, we have the square toroid.

approach ideally suits for step-up applications with over-chip integration. An inductance per unit area of ~2 µH/mm^2 up to 1 MHz (and inductance per unit core volume of ~15.6 µH/mm^3) has been obtained along with an inductance to DC resistance ratio of 2.23 µH/Ω, appropriate for the development of low voltage micro-power EH systems and PwrSiP and PwrSoC.

The paper has also shown additional optimization techniques showing that there exists an optimum core width that maximizes the inductance value once the footprint area has been fixed. Planar square toroidal inductors can achieve the same permeance value of an equivalent round toroid, but using a smaller footprint area and a lower profile. Serpentine core inductors can overcome the limits of the square toroid by spreading the core all over the surface with a serpentine geometry. Such layout is suitable in case a high-resolution patterning technique is available, but its application for high numbers of meanders might be practically limited by constraints of wire bonder machines.

Future investigations include the fabrication of more compact structures to enhance further the coupling and the turns ratio, and the use of flip-chip bonding as an alternative to wire bonding process to fabricate the top conductors, as well as new layouts for planar cores to be used in on-chip and over-chip implementations.

References

[1] C. O. Mathúna, N. Wang, S. Kulkarni, and S. Roy, "Review of integrated magnetics for power supply on chip (PwrSoC)", *IEEE Trans. Power Electron.*, vol. 27, no. 11, pp. 4799-4816, (2012).

[2] J.-P. Im, S.-W. Wang, S.-T. Ryu, and G.-H. Cho, "A 40 mV Transformer-reuse self-startup boost converter with MPPT control for thermoelectric energy harvesting", *IEEE J. of Solid-State Circ.*, vol. 47, no. 12, pp. 3055-3067, (2012).

[3] P.-S. Weng, H.-Y. Tang, P.-C. Ku, and L.-H. Lu, "50 mV-Input batteryless boost converter for thermal energy harvesting", *IEEE J. of Solid-State Circ.*", vol. 48, no. 4, pp.1031-1041, (2013).

[4] E. Macrelli, A. Romani, N. Wang, S. Roy, M. Hayes, and R. P. Paganelli, C. Ó Mathúna, M. Tartagni, "Modeling, design, and fabrication of high inductance bond wire micro-transformers with toroidal ferrite core", *IEEE Trans. Power Electron.*, vol. 30, no. 10, pp. 5724-5737, (2014).

[5] E. Macrelli, A. Romani, R.P. Paganelli, A. Camarda, M. Tartagni "Design of Low-Voltage Integrated Step-up Oscillators with Microtransformers

for Energy Harvesting Applications", *IEEE Trans. Circ. and Syst.—I: Reg. Pap.* (*TCAS*)., vol. 62, no. 7, pp. 1747-1756 (2015).

[6] B. Razavi, "Design of analog CMOS integrated circuits". McGraw-Hill International Ed., (2001).

[7] M. K. Kazimierczuk, High-Frequency Magnetic Components, second edition, John Wiley & Sons, (2014).

[8] C. R. Sullivan, D. V. Harburg, J. Qiu, C. G. Levey, and D. Yao, "Integrating magnetics for on-chip power: a perspective", *IEEE Trans. Power Electron.*, vol. 28, no. 9, pp. 4342-4353, (2013).

[9] R. Meere, N. Wang, T. O'Donnell, S. Kulkarni, S. Roy, and S. C. O'Mathuna, "Magnetic-core and air-core inductors on silicon: a performance comparison up to 100 MHz", *IEEE Trans. Magn.*, vol. 47, no. 10, pp. 4429-4432, (2011).

[10] Q. Li, M. Lim, J. Sun, A. Ball, Y. Ying, F. C. Lee, and K. D. T. Ngo, "Technology roadmap for high frequency integrated DC-DC converter", *Proc. Power Electron. Motion Control Conf.*, pp. 1-8, (2009).

[11] B. Orlando, R. Hida, R. Cuchet, M. Audoin, B. Viala, D. Pellissier-Tanon, X. Gagnard, and P. Ancey, "Low-resistance integrated toroidal inductor for power management", *IEEE Trans. Magn.*, vol. 42, no. 10, pp. 3374-3376, (2006).

[12] E. Macrelli, N. Wang, S. Roy, M. Hayes, R. P. Paganelli, M. Tartagni, and A. Romani, "Design and fabrication of a 315 μH bondwire micro-transformer for ultra-low voltage energy harvesting", *Proc. Design, Automation and Test in Europe COnf* (DATE), Dresden, DE, pp.1-4, (2014).

[13] E. Macrelli, A. Romani, N. Wang, S. Roy, M. Hayes, R. P. Paganelli, and M. Tartagni. "Design and fabrication of a 29 μH bondwire micro-transformer with LTCC magnetic core on silicon for energy harvesting applications." Procedia Engineering 87 (2014): 1557-1560.

[14] A. C. Fischer, J. G. Korvink, N. Roxhed, G. Stemme, U. Wallrabe, F. Niklaus, "Unconventional applications of wire bonding create opportunities for microsystem integration", *J. of Microm. and Microeng.*, Vol. 23, n 8, article id. 083001 (2013).

[15] J. Lu, H. Jia, A. Arias, X. Gong, and Z. J. Shen, "On-chip bondwire transformers for power SOC applications", *Proc. Appl. Power Electron. Conf.*, pp. 199-204, (2008).

[16] J. Lu, H. Jia, X. Wang, K. Padmanabhan, W. G. Hurley, and Z. J. Shen, "Modeling, design, and characterization of multiturn bondwire inductors with ferrite epoxy glob cores for power supply system-on-chip or system-in-package applications", *IEEE Trans. Power Electron.*, vol. 25, no. 8, pp. 2010-2017, (2010).

[17] X. Yu, J. Kim, F. Herrault, M. G. Allen, "Silicon-Embedded Toroidal Inductors with Magnetic Cores: Design Methodology and Experimental Validation", 2014 IEEE *Appl. Pow. Electr. Conf. and Exp.* (APEC), pp. 763-767.

[18] Y. M. Nguyen, T. Lopez, J.-P. Laur, D. Bourrier, S. Charlot, Z. Valdez-Nava, V. Bley, C. Combettes, and M. Brunet, "Soft ferrite cores characterization for integrated micro-inductors", *J. of Physics: Conf. Series*, vol. 476, no. 1, p. 012139. *IOP Publishing* (2013).

[19] Y. M. Nguyen, D. Bourrier, S. Charlot, Z. Valdez-Nava, V. Bley, C. Combettes, T. Lopez, J.-P. Laur, M. Brunet, "Soft ferrite cores characterization for integrated micro-inductors", *J. of Micromech. and Microeng.*, vol. 24, no. 10, doi: 10.1088/0960-1317/24/10/104003.

[20] P. L. Fulmek, P. Haumer, I. Atassi, B. Schweighofer, and H. Wegleiter, "Magnetic DC-properties of LTCC-ferrite material and their temperature dependence", *IEEE Trans. Magn,* vol. 48, no. 4, pp. 1541-1544, (2012).

[21] C. R. Sullivan, W. Li, S. Prabhakaran, and L. Shanshan, "Design and fabrication of low-loss toroidal air-core inductors", *Proc. Appl. Power Electron. Conf.*, pp. 1754-1759, (2007).

[22] M. Franz, K. Makarovic, S. Lüftl, A. Maric, I. Atassi, M. Hrovat, N.Blaz, G. Radosavljevic, "Characterization and binder burnout studies of ferrite LTCC tapes", *Proc. 36th Intern. Spring Seminar on Electr. Techn.* (2013).

[23] J. Wang, Flexible on-chip inductors and transformer, *Proc. IMAPS Device Packaging Conf.*, Mar. 2010.

[24] M. Mu, W. Zhang, F. C. Lee, and Y. Su, "Laminated low temperature co-fired ceramic ferrite materials and the applications for high current POL converters", *Proc. Energy Convers. Congress and Exposition*, Denver, CO, pp. 621-627, (2013).

[25] ESL 40012 datasheet. Link: http://www.electroscience.com/pdf/40012.pdf

[26] A. H. Feingold, M. Heinz, R. L. Wahlers, and M. Stein, "Materials for capacitive and inductive components integrated with commercially available LTCC systems", in *Proc. IMAPS* Israel (2003), link: http://electro-science.com/publications/2003_imaps_israel.pdf.

[27] A. Shamim, J. Bray, L. Roy, N. Hojjat, R. A. Elasoued, D. Baillargeat, "Microwave and magnetostatic characterization of ferritic LTCC for tunable and reconfigurable SiP applications," in *Proc.IEEE/MTT-S*, *Int. Microwave Symp*. (2007), Honolulu, HI, pp. 691-694.

[28] N.Blaz, A. Maric, G. Radosavljevic, L. Zivanov, "Determination of electric and magnetic properties of commercial LTCC soft ferrite material", *J. of Microelectr. and Electr. Pack.* (2011) 8(1), pp.1-9.

[29] N.Blaz, A. Maric, G. Radosavljevic, L. Zivanov, G. Stojanovic, "Modeling and characterization of frequency and temperature variation of complex permeability of ferrite LTCC Material", *Progress In Electromagn. Res. B* (2010), vol. 23, pp. 131-146.

[30] N.Blaz, A. Maric, I. Atassi, G. Radosavljevic, L. Zivanov, H. Homolka, W. Smetana, "Complex permeability changes of ferritic LTCC samples with variation of sintering temperatures", *IEEE Trans.Magn.,* vol. 48, no. 4, pp.1563-1566, (2012).

[31] W. H. Preece, "On the heating effects of electric currents", *Proc. Royal Society of London,* 36.228-231, pp.464-471, (1883).

[32] K.H.J. Buschow, "Handbook of magnetic materials", Chap. 3 Nanocrystalline soft magnetic alloys, 1997 Elsevier Science, pp. 415-462.

[33] C. R. Sullivan, "Overview of core loss prediction (dtthi) (and measurement techniques) for non-sinusoidal waveforms", APEC 2012 presentation.

[34] J. Li, T. Abdallah, C. R. Sullivan, "Improved Calculation of Core Loss With Nonsinusoidal Waveforms", Industry Applications Conference, 2001. *Thirty-Sixth IAS Annual Meeting. Conference Record of the 2001 IEEE*, pp. 1-8.

[35] M. Mu, "High Frequency Magnetic Core Loss Study", Ph.D. dissertation, Virginia Polythecnic Institute, 2013.

[36] C. J. Dunlop, "Modeling Magnetic Core Loss for Sinusoidal Waveforms", M. Sc. Dissertation, Massachussets Institute of Technology (MIT) – 2008.

[37] J. G. Hayes, D. Cashman, M. G. Egan, T. O'Donnell, and N. Wang, "Comparison of test methods for characterization of high-leakage two-winding transformers", *IEEE Trans. Ind. Appl.*, vol.45, no .5, pp. 1729-1741, (2009).

[38] A. Camarda, A. Romani, M. Tartagni, "Piezoelectric transformers for ultra-low voltage energy harvesting applications", *Procedia Eng.* Vol. 87 pp. 1521–1524 (2014).

[39] A. Camarda, A. Romani, E. Macrelli, M. Tartagni, "A 32 mV/69 mV input voltage booster based on a piezoelectric transformer for energy harvesting applications", *Sens. Actuators A: Phys.* (2015), Vol. 232, pp. 341-352 (2015).

[40] A. Camarda. M. Tartagni, A. Romani, "A -8 mV/+15 mV Double Polarity Piezoelectric Transformer-Based Step-Up Oscillator for Energy Harvesting Applications", *IEEE Trans. Circ. and Syst.—I: Reg. Pap.* (*TCAS*) (in press), doi: 10.1109/TCSI.2017.2741779.

[41] A. Romani, A. Camarda, A. Baldazzi, M. Tartagni, "A Micropower Energy Harvesting Circuit with Piezoelectric Transformer-Based Ultra-low Voltage Start-up", *IEEE Int. Symp. Low Pow. Electron. Des.* (*ISLPED*), pp. 279-284 (2015).

[42] Coilcraft, Miniature step-up flyback transformers - LPR4012, 2010. url: http://www.coilcraft.com/pdfs/lpr4012.pdf.

[43] Coilcraft. Miniature step-up flyback transformers - LPR6235. 2010. url: http://www.coilcraft.com/pdfs/lpr6235.pdf.

[44] A. Camarda, E. Macrelli, A. Romani, M. Tartagni, "Design Optimization of Integrated Magnetic Core Inductors", *IEEE Trans. Magn*., vol. 51, no. 7, (2015) id: 8401010.

This article has been accepted for publication in a future issue of this journal, but has not been fully edited. Content may change prior to final publication. Citation information: DOI 10.1109/JESTPE.2017.2751745, IEEE Journal of Emerging and Selected Topics in Power Electronics

Antonio Camarda received the B. Sc. And M.S. degree in Electronic Engineering from the Polytechnic University of Bari, Bari, Italy, in 2006 and 2010 respectively. He has then been working in the ICT field a year and a half. In 2011 he joined the research lab University of Bologna –ST Microelectronics as a free-lance analog IC designer. In 2013 he was selected for the PhD program. In 2015 he joined the Vienna University of Technology as visiting PhD student for the fabrication of MEMS piezoelectric transformers. He gained his Ph.D. degree from the University of Bologna in 2016 with a dissertation in the More than Moore context, focused on the integration of both Magnetic and Piezoeletric devices together with the ICs. His research interests include modeling and design of piezoelectric devices, micro-power ICs, energy harvesting systems, ultra-low voltage start-up techniques and resonant power conversion systems.

Enrico Macrelli received the B.S. and M.S. degrees in electronic engineering, in 2007 and 2009, respectively, and the Ph.D. degree in information technology, in 2014, all from the University of Bologna, Italy. In 2015 he joined the Department of Electrical and Computer Engineering, National University of Singapore, where he is currently a Research Fellow. In 2012, he was Research Intern at the Tyndall National Institute, Cork, Ireland. His research interests include design and modeling of integrated gas sensors and low-power interfaces, micromagnetic and piezoelectric materials and devices, and startup integrated circuits for micropower energy harvesting.

Rudi Paolo Paganelli received the Dr. End. degree in Electrical Engineering and electrical engineering and Ph.D. degree in electrical engineering, computer science, and telecommunications from the University of Bologna, Bologna, Italy, in 1998 and 2002, respectively. In 2002, he joined the CNR-IEIIT, Bologna, Italy, as a Research Fellow, and since 2003, has been as an Assistant Professor of the course on power electronics with the University of Bologna. His research interests include electronic device modeling, microwave circuit design, nonlinear circuits, and power electronics.

Marco Tartagni received an M.S. in Electrical Engineering and a Ph.D. in Electrical Engineering and Computer Sciences both from the University of Bologna, Italy. During his Ph.D. program, he joined the Department of Electrical Engineering at the California Institute of Technology in 1992 as a visiting student and in 1994 as a research fellow. Since March 1995 he has been with the Department of Electronics, Bologna University, where he is currently an Associate Professor. From 1996 to 2001 he was team leader in the joint STMicroelectronics and Bologna University lab. He was co-recipient of the Van Vessem Outstanding Paper Award, received at the 2004 IEEE ISSCC conference. He has been local and European coordinator of several FP5-6-7 projects in the Nanotechnology and ICT thematic areas. In 2008 he has been coordinator of the Energy Autonomous Systems of the European CATRENE initiative. Since 2014 he is member of the scientific board and team leader of the joint STMicroelectronics and Bologna University lab for sensor design. He is author or co-author of more than 100 peer-reviewed scientific publications in the field of sensor theory, design and testing. He is also the holder of 18 US and 11 European and WIPO granted patents.

Prof. **Saibal Roy** is currently a Research Professor in the department of Physics, University College Cork (UCC), Ireland and Head of Micropower Systems and Nanomagnetics in Tyndall National Institute, Ireland. He is holding Science Foundation Ireland (SFI) PI grant award and also a funded investigator in SFI €39 Million research center on 'Internet of Things - CONNECT'. He is well known internationally particularly in the area of integrated high frequency magnetics for power supply on chip, vibrational energy harvesting through electromagnetic transduction (EMT) and demonstrating unconventional properties in different magnetic nano-hetero-structures. Within the last decade, Prof. Roy was able to bring over €7Million competitive direct research grants focusing these areas. Some of his published works on 'Miniaturized/MEMS vibrational energy harvesting through EMT' have received numerous citations and featured widely in international media. On the other hand, Tyndall 'Magnetics on Si' team successfully licensed the micro-transformer/inductor technology recently with a substantial license fee to two major multinational companies. In recognition, the team was awarded as the research team of the year (2015) by the University. Recently, Prof. Roy was awarded the 'A. S. Paintal visiting Chair Professorship' in Engineering by INSA (Indian National Science Academy) to visit most premier academic/research institutions in India. Prof. Roy has 3 global patents, written 7 book chapters and published over 170 papers in leading journals and conference proceedings, which have resulted in > 4000 international citations with h index of 31, to date.

Aldo Romani received the Dr. Eng. degree in Electrical Engineering in 2001 and the Ph.D. degree in Electrical Engineering, Computer Science and Telecommunications in 2005 from the University of Bologna (Italy), where he currently serves as associate professor. He has been involved with CMOS integrated sensors, applications of piezoelectric materials, and energy harvesting systems. He has authored or co-authored more than 60 international scientific publications. Dr. Romani was a co-recipient of the 2004 Jan Van Vessem Award of the IEEE International Solid-State Circuits Conference.